

Stress distribution in two-dimensional silos

Rodolfo Blanco-Rodríguez and Gabriel Pérez-Ángel

Departamento de Física Aplicada, Centro de Investigación y de Estudios Avanzados del Instituto Politécnico Nacional, Unidad Mérida. Apartado Postal 73 “Cordemex” 97310, Mérida, Yucatán, México

 (Received 24 July 2017; revised manuscript received 20 December 2017; published 10 January 2018)

Simulations of a polydispersed two-dimensional silo were performed using molecular dynamics, with different numbers of grains reaching up to 64 000, verifying numerically the model derived by Janssen and also the main assumption that the walls carry part of the weight due to the static friction between grains with themselves and those with the silo’s walls. We vary the friction coefficient, the radii dispersity, the silo width, and the size of grains. We find that the Janssen’s model becomes less relevant as the silo width increases since the behavior of the stresses becomes more hydrostatic. Likewise, we get the normal and tangential stress distribution on the walls evidencing the existence of points of maximum stress. We also obtained the stress matrix with which we observe zones of concentration of load, located always at a height around two thirds of the granular columns. Finally, we observe that the size of the grains affects the distribution of stresses, increasing the weight on the bottom and reducing the normal stress on the walls, as the grains are made smaller (for the same total mass of the granulate), giving again a more hydrostatic and therefore less Janssen-type behavior for the weight of the column.

DOI: [10.1103/PhysRevE.97.012903](https://doi.org/10.1103/PhysRevE.97.012903)

I. INTRODUCTION

Many industrial processes require storing bulk solids (grains) and the containers used for their storage are called silos. When a silo fails, it can be devastating [1]. The design of silos requires a depth analysis of the grain-silo system, therefore, the estimation of stresses is critical to their design. For a granular system, the intergrain forces are entirely classical, consisting of contact force. Stress chains, stable arcs, and voids are generated in a silo, so that a vertical load may generate a significant horizontal component [2,3]. Contrary to the normal hydrostatic situation, the pressure at the base of the silo does not increase indefinitely as the height of the material inside it is increased. The pressure at the bottom saturates at a certain height. The first to study this phenomenon was Roberts in 1884; he noted that the pressure at the bottom ceases to increase when the height of the granular column is twice the diameter of the inscribed circle in the base. In 1895, the German engineer Janssen proposed a model describing the redirection of forces toward the walls. He derived the equivalent of the barometric formula for granular material from the main assumption that the walls carry part of the weight [4,5]. The model rests on three principles:

- (i) The medium is treated as though it was continuous.
- (ii) A vertical stress applied to the granular material automatically generates a proportional horizontal stress such that $\sigma_h = K\sigma_v$.
- (iii) The frictional force between the particles and the walls is at the point of Coulomb failure: $F_s = \mu_w F_n$, where F_s and F_n are the magnitudes of the tangential friction force and normal force at the wall, respectively, with static friction coefficient grain-wall μ_w .

The Janssen’s model predicts the vertical stress σ_{zz} at the bottom in a two-dimensional grains system with bulk density

ρ_b in a silo of width L as

$$\sigma_{zz}^{\text{Jan}} = \frac{\rho_b g L}{2\mu_w K} (1 - e^{-2\mu_w K z/L}), \quad (1)$$

where g is the gravitational acceleration and z is the depth measurement, starting from the upper surface. Currently, several studies have explored the limits of the Janssen’s model: Vanel *et al.* [6] reported precise and reproducible measurement on the static pressure at the bottom of a granular column, showing the limit of the classical Janssen’s model and making a simple extension by introducing an effective hydrostatic zone in the upper part of the granular column. On the other hand, de Gennes [7] mentioned that although Janssen proposed a constant ratio between horizontal and vertical stress, $\sigma_{rr} = K\sigma_{zz}$ in cylindrical coordinates, a granular system in certain states of compaction will show a resistance to compression measured by a macroscopic bulk modulus K (which is the same K that appears in Janssen’s formula); since the forces are mediated by small contact regions between two adjacent grains and the contact areas increase with pressure, K will increase with pressure. As the material in a silo is under compression everywhere, in those situations the granular medium may be described as a quasielastic medium where one gets $K = \sigma_p/(1 - \sigma_p)$ with σ_p the Poisson ratio of the material. In a different approach, Vanel *et al.* [8] mentioned a simple hyperbolic model (called “oriented stress linearity”) giving a fundamental role to the network of force chains; this model considers $\sigma_{rr} = \eta_1 \sigma_{zz} + \eta_2 \sigma_{rz}$ with $\eta_{1,2}$ depending of the orientation of the force chains.

The friction coefficient between grains and walls is a decisive parameter in the Janssen’s model. Landry *et al.* [9] studied granular packing using large-scale discrete element computer simulations in two- and three-dimensional domains, showing the effective hydrostatic zone and finding that the

interior of the packing is far from the Coulomb failure, while the forces at the walls are close to it. Bertho *et al.* [10] reported measurements at the bottom of granular packings inside a vertical tube in relative motion, showing that the grain packing reaches a dynamical equilibrium independently of the initial state and of the relative velocity with respect to the walls. Also, a state of nonhomogeneous friction fully characterized by a generalized frictional coefficient dependent of the depth $\mu(z)$ has been studied in [11].

The most difficult parameter to test in the Janssen's model is the factor K (known as the coefficient of earth pressure at rest “ K_0 ” in geotechnical field); the dependence of Janssen's factor on the particle characteristics is mainly unknown. In practice, the Jaky's equation is the most widely used to estimate K , relating it with the effective internal friction angle ϕ' as $K = 1 - \sin \phi'$; this definition implies that K is unique for each type of granular material and independent of the initial state; nevertheless, this equality fails in certain situations. Lee *et al.* [12] measured K for sand particles and glass beads under various conditions and found that denser sand showed lower K values, that they attributed to the development of strong force chains in the vertical direction, which leads to lower degrees of stress transmission in the horizontal direction. They also tested the effect of the particle shape and found that Jaky's equation was valid for uniformly round glass beads but not for sand (irregular shape). The most popular method of experimental determination of K is the uniaxial compression test, which has been used to measure the ratio of lateral to vertical pressure of different cereal grains. For these experiments, K ranged from 0.37 to 0.74 [13]. While K is expected to range from 0 to 1, values larger than 1 have been found. In [14], a measure of the pressure at the bottom for different amounts of glass spheres in a smooth Perplex column was performed. The authors' fit is in agreement with the Janssen approach; they considered a friction coefficient of 0.13 between glass-Perplex and found $K = 1.7$. Numerical simulations have allowed to study K to grain level; Wiącek *et al.* [15] showed that the degree of polydispersity of a granular assembly determines strongly the average coordination number (number of contacts per particle), however, the macromechanical response to applied compressive pressure depends only slightly on particle size heterogeneity. Lopera *et al.* [16] evidenced the dependency of K with void ratio; K increases as void ratio increases. Similar observations were reported by Gu *et al.* [17]; they also found that K decreases as the coordination number increases and revealed that the particle rearrangement is negligible when the vertical stress approaches the maximum value. Recently, Khalili *et al.* [18] studied one-dimensional compression of granular materials with systems prepared in both isotropic and anisotropic configurations, differing in solid fraction and coordination number. They showed that K depends on the initial state of the granular assembly: it is related to the evolution of internal variables and it may exceed the value 1 in unloading.

In this work, we investigate the behavior of K when the friction coefficient, polydispersity, size of silo, and size of grains are varied. The silo's bottom was slowly moved down, with three purposes: (1) to simulate the experiments in [10], (2) to use the fact that the frictional forces with the walls are mobilized and demobilized from time to time, changing the

history of the system and increasing the statistics, and (3) to drive the granulate to be close to the point of Coulomb failure, improving the contact between Janssen's model and the simulation. Also, we study the large bottom limit of the silo, which for a given grain size may begin to show some quasihydrostatic effects. Finally, we compare the effect of varying the grain average radius keeping the size of silo with that of varying the size of silo keeping the grain average radius, finding some unexpected results.

II. SIMULATION METHOD

The numerical simulation was performed with codes written in CUDA-C and using molecular dynamics, including the effects of the static friction via the Cundall-Strack approximation [19,20] and a modified velocity-Verlet algorithm to integrate the motion equations. A two-dimensional system was configured, simulating different numbers of grains as disks with three degrees of freedom (two translational and one rotational), and radius $R_\alpha = R_{\text{ave}} + a\Delta R$, where R_{ave} is the average radius, ΔR is the maximum fluctuation, and a is a random number chosen between -1 and 1 with uniform distribution. The container was rectangular with adjustable width and indefinite height, the walls (perfectly rigid) obey the same rules of interaction as the disks of the system.

The contact force between a disk α and a disk β is decomposed into normal and tangential components $\mathbf{F}_{\alpha\beta} = \mathbf{F}_n + \mathbf{F}_s$. The normal force is described by a spring-dashpot model considering that the disks experience a relative normal compression in the vicinity of contact point given by

$$\xi = \max(0, R_\alpha + R_\beta - |\mathbf{r}_\beta - \mathbf{r}_\alpha|), \quad (2)$$

and the magnitude of the normal force is defined as

$$F_n = \min(0, -k_n\xi - \gamma_n\dot{\xi}), \quad (3)$$

where k_n and γ_n are elastic and viscoelastic constants, respectively. It should be noticed that the real life realization of the two-dimensional model used here implies an aggregate of short parallel cylinders (for example, coins between two close flat boundaries), which makes quite cumbersome to implement a more realistic contact force; from the point of view of elastic theory, this is a Hertz-type force. For the parallel contact between two cylinders, see [21].

The tangential component is due to dry frictional forces between disks that include a cinematic friction and a static friction. The cinematic friction is proportional to the normal force as μF_n . To implement the static friction, we used the Cundall-Strack approach, where it is assumed that it can be represented by a stiff spring whose elongation is given by the tangential displacement ζ accumulated from the instant of contact t_0 :

$$\zeta = \int_{t_0}^t v_s(t') \Theta[\mu F_n/k_s - |\zeta(t)|] dt', \quad (4)$$

where k_s is elastic constant, and the Heaviside function is used to control the growth of ζ [20]. Following the spring-dashpot model, the magnitude of the tangential force can be defined as

$$F_s = -\min(|k_s\zeta + \gamma_s\dot{\zeta}|, |\mu F_n|) \text{sgn}(\zeta), \quad (5)$$

with viscoelastic constant γ_s . We configure the viscoelastic and elastic constants, respectively, as

$$\gamma_n = \frac{1}{5}\gamma_s = -\frac{m_{\text{ave}} \log e_n}{t_{\text{coll}}}, \quad (6)$$

$$k_n = k_s = \frac{m_{\text{ave}}}{2} \left(\frac{\pi^2}{t_{\text{coll}}^2} + \frac{\gamma_n^2}{m_{\text{ave}}^2} \right), \quad (7)$$

where $m_{\text{ave}} = \rho\pi R_{\text{ave}}^2$ is the average disk mass with density ρ , e_n is the normal restitution constant, and t_{coll} is the collision time between two disks, both for typical situations [22]. The simulations were run with fixed physical parameters: $\rho = 4.0 \text{ g/cm}^2$, $t_{\text{coll}} = 10^{-4} \text{ s}$, and $e_n = 0.5$.

To integrate the motion equations, we used the velocity-Verlet algorithm with a predictor-corrector modification, introduced to account for the velocity dependence of the force. The global form is

$$\begin{aligned} \mathbf{r}(t + dt) &= \mathbf{r}(t) + \mathbf{v}(t)dt + \frac{1}{2}\mathbf{a}(t)dt^2, \\ \mathbf{v}_p(t + dt) &= \mathbf{v}(t) + \mathbf{a}(t)dt, \\ \mathbf{a}(t + dt) &= \frac{1}{M}\mathbf{F}(\mathbf{r}(t + dt), \mathbf{v}_p(t + dt)), \\ \mathbf{v}(t + dt) &= \mathbf{v}_p(t) + \frac{1}{2}[\mathbf{a}(t + dt) - \mathbf{a}(t)]dt, \end{aligned} \quad (8)$$

where \mathbf{r} , \mathbf{v} , \mathbf{a} , \mathbf{F} are position, velocity, acceleration, and force vectors, respectively, and M is the mass or inertia moment of a particle [23]. The time step used in the simulations was $dt = t_{\text{coll}}/150$.

The Janssen's model assumed that the frictional force between the particles and the wall are at the point of Coulomb failure. In this work, the base of the silo was slowly moved downward with velocity $v_b = 0.001\sqrt{4gR_{\text{ave}}}$ to mobilize the frictional forces between grains and walls [10]; the process ends up generating occasional internal avalanches, which allows us to study the particle-wall interaction at all stages before Coulomb failure.

Although for the practical design of silos the most important part is the stress (in particular, normal stress) on the walls, it is also interesting to study the internal distribution of stresses. In the simulations, the stress tensor was defined as [24]

$$\sigma_{ij} = \frac{1}{A} \sum_{C_{\alpha\beta} \in A} F_i^{C_{\alpha\beta}} b_j^{C_{\alpha\beta}}, \quad (9)$$

where the sum is performed over the contact points $C_{\alpha\beta}$ inside a previously defined cell of area A (large enough to fit 20 cells across the width of the silo), $\mathbf{F}^{C_{\alpha\beta}}$ is the interaction force between the grains α - β in $C_{\alpha\beta}$, $\mathbf{b}^{C_{\alpha\beta}} = \mathbf{r}_\alpha - \mathbf{r}_\beta$ is the vector connecting the centers of the grains α - β , and the subscripts i and j indicate Cartesian components [25]. For internal stress considerations, the contact wall-grain was considered as two grains of the same size in contact with each other.

III. DESCRIPTION OF THE TESTS

The silo width, the friction coefficient, and the dispersity radius were varied for each simulation. The initial positions were in an hexagonal mesh with a little more than one maximum diameter of distance between centers of the grains

to avoid the overlapping of grains; the radii had a uniform and random dispersion; each grain had an initial velocity $v_0 = 1.0 \text{ cm/s}$ in random direction. The grains fall by gravity towards a static base; after some time, when the grains are static, the base is slowly moved downward. The movement of the base tends to eliminate much of the influence of the initial condition, due to internal avalanches.

To test the algorithms, a static silo was run and the kinetic energy was obtained. After $\sim 10^6$ time steps, the total kinetic energy decayed to $\sim 10^{-19} \text{ J}$, which compared to the scale of kinetic energy $\sim 10^{-4} \text{ J}$ (one particle falling by gravity a distance of one diameter) can be considered zero. The use of variables with double precision was necessary to obtain these values.

In the first series of simulations, we considered a silo width $L = 20 \text{ cm}$, grains with $R_{\text{ave}} = 0.5 \text{ cm}$ and $\Delta R = 0.10 \text{ cm}$. The friction coefficients grain-grain and wall-grain were the same, $\mu_w = \mu$, and for this series we tested the values $\mu = 0.2, 0.4, 0.6$, and 0.8 . The simulations were run with different numbers of grains, reaching up to 4000 in steps of 200, using 9×10^6 time steps. Other simulations were performed in the same way but with a fixed friction coefficient $\mu = 0.6$ and $\Delta R = 0.10, 0.20, 0.25$, and 0.30 cm .

The next series of simulations was performed with silo widths $L = 40, 60$, and 80 cm , friction coefficient $\mu = 0.6$, $\Delta R = 0.10$, $R_{\text{ave}} = 0.5 \text{ cm}$, and the same type of initial conditions. For the simulations of width $L = 40 \text{ cm}$, the maximum number of the grains reached was 16 000 in steps of 800, using 12×10^6 time steps. For $L = 60 \text{ cm}$, the maximum number of grains reached was 36 000 in steps of 1800, using 15×10^6 time steps. For $L = 80 \text{ cm}$, the maximum number of grains reached was 64 000 grains in steps of 3200, using 18×10^6 time steps.

Finally, a series of simulations were performed with friction coefficient and time steps same as the previous and the total mass was kept fixed. The average radii were varied to $R_{\text{ave}} = 0.5, 0.25, 0.167$, and 0.125 , for a maximum number of grains equal to 4000, 16 000, 36 000, and 64 000 grains, respectively. All these simulations kept a 20% dispersity of the radii.

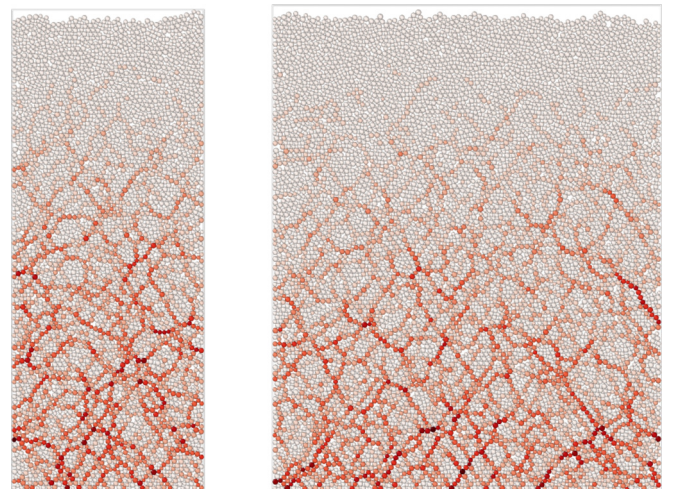


FIG. 1. Force chains in silos with 4000 grains (left) and 8000 grains (right). Here, we use $\mu = 0.6$.

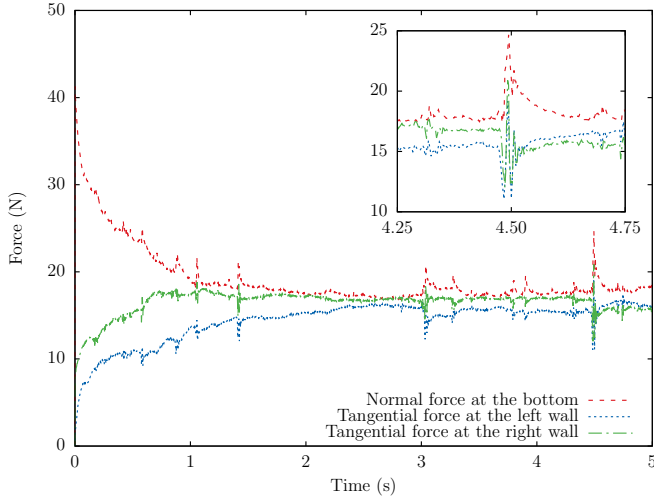


FIG. 2. Forces on the lateral walls and base of the silo as a function of time, starting from the moment when the base starts to slide down. This is a typical behavior of forces for 1600 grains and $L = 20$ cm. A zoom view of the peaks due to internal avalanches is displayed. We can observe that the peaks in the tangential force on the walls are synchronized to the normal force on the bottom, although with different sign. Notice that in general the tangential force in the left and right walls is close but different, and that the avalanches affect both sides of the silo simultaneously.

The simulations were performed on a cluster computer with GPU acceleration using graphic cards NVIDIA Tesla K20 and K40. A typical simulation with 64 000 grains and 18×10^6 time steps takes ~ 24 h. The simulations were observed with the open visualization tool OVITO [26,27], where the force chains can be seen. An example is displayed in Fig. 1.

IV. RESULTS

Each simulation was run 16 times with different random initial velocities and radii distribution, and we collected the normal and tangential force on the walls, the normal force on the base, the time and height distribution of forces over the wall, and the internal stress matrix of the granular column. In Fig. 2 we show the forces on the lateral walls and base of the silo starting when the base starts to slide down. The tangential force on the walls already exceeds the normal force on the bottom for one simulation of 1600 grains. This indicates that most of the weight of the granular column is carried by the walls. The forces are in phase and it should be noted that well defined peaks appear from time to time. The downward motion of the base induces internal avalanches, and therefore the granular column is subjected to a compression-decompression cycle. Notice that the weight carried by the base reaches the saturation (even moving downward) and is smaller than the saturation of the weight on the static base (that is, at beginning of the simulations); this confirms the experimental measurements in [10]. It should be noticed, however, that the resolution achieved in the experiments does not seem to be enough to show the internal avalanches.

After a transient time, the normal stress on the base of the silo was averaged and fitted to a modified Janssen's model with

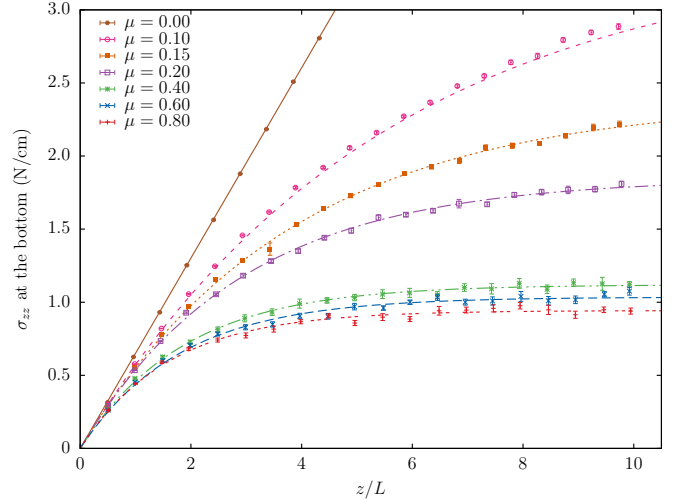


FIG. 3. Vertical stress σ_{zz} on the bottom for a silo of width $L = 20$ cm, with different values of friction coefficient μ . The points are averages over 16 runs. The lines are the fits to the Janssen's model. A perfect hydrostatic behavior can be observed when there is no friction ($\mu = 0.0$). Notice, however, in Table I that α becomes clearly smaller than 1 for larger values of μ . Full fit data in Table I.

the free parameter K and a parameter of proportionality α , such that $\sigma_{zz} = \alpha \sigma_{zz}^{\text{Jan}}$ (with $\alpha = 1$ we have the original Janssen's model). The two-dimensional bulk density was calculated with the total mass of the grains and the area of the final granular column, obtaining an average value of $\rho_b = 3.23 \pm 0.02$ g/cm². For lower values of friction coefficient, higher values of the dispersity of the radii or larger bases, we obtained slightly higher values of bulk density.

TABLE I. Fit parameters for the simulated silos.

Parameters of simulation	K	α
$L = 20$ cm; $\Delta R = 0.1$ cm		
$\mu = 0.10$	0.92 ± 0.01	1.00 ± 0.01
0.15	0.87 ± 0.01	0.99 ± 0.01
0.20	0.86 ± 0.01	1.00 ± 0.01
0.40	0.66 ± 0.01	0.95 ± 0.02
0.60	0.46 ± 0.01	0.91 ± 0.02
0.80	0.39 ± 0.01	0.94 ± 0.03
$L = 20$ cm; $\mu = 0.6$		
$\Delta R = 0.10$ cm		
0.10 cm	0.46 ± 0.01	0.91 ± 0.02
0.20 cm	0.55 ± 0.02	0.99 ± 0.03
0.25 cm	0.53 ± 0.02	0.95 ± 0.03
0.30 cm	0.49 ± 0.03	0.88 ± 0.05
$\Delta R = 0.10$ cm; $\mu = 0.6$		
$L = 20$ cm	0.46 ± 0.01	0.91 ± 0.02
40 cm	0.36 ± 0.01	0.87 ± 0.02
60 cm	0.24 ± 0.01	0.80 ± 0.02
80 cm	0.16 ± 0.01	0.72 ± 0.02
$L = 20$ cm; $\mu = 0.6$		
$R = 0.500 \pm 0.100$ cm	0.46 ± 0.01	0.91 ± 0.02
0.250 ± 0.050 cm	0.35 ± 0.02	0.84 ± 0.03
0.167 ± 0.033 cm	0.19 ± 0.01	0.71 ± 0.03
0.125 ± 0.025 cm	0.17 ± 0.01	0.72 ± 0.02

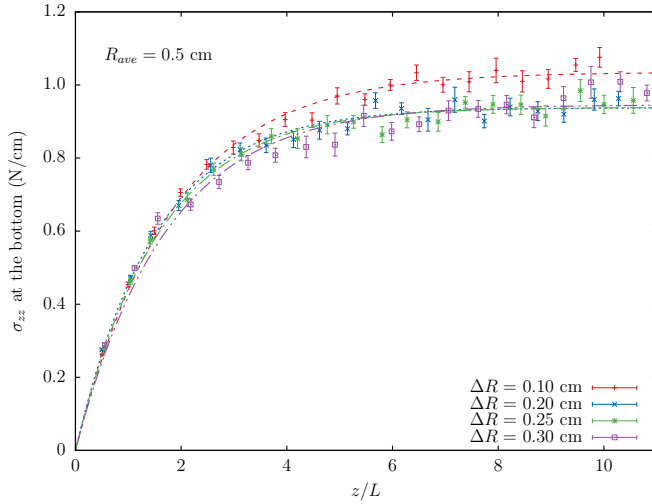


FIG. 4. Vertical stress σ_{zz} on the bottom for a silo of width $L = 20$ cm, with $\mu = 0.6$, and different values of dispersity of the radii. The points are averages over 16 runs. The lines are the fits to the Janssen's model. The granular columns for larger ΔR are a bit higher than for smaller ΔR , although their bulk densities are similar. We obtained similar fits for larger dispersity of radii; the smallest ΔR has a weight of saturation a bit higher. Full fit data in Table I.

A. Varying the friction coefficient

Figure 3 shows the vertical stress σ_{zz} for different friction coefficients, where the Janssen profile can be clearly noted. Due to the fact that the walls carry part of the weight by frictional forces, systems with lower friction coefficient reach a saturation stress greater than the systems with higher friction coefficients. Also, we can observe the inverse relation between the saturation of vertical stress and the friction coefficient, although for values of friction coefficient greater than 0.5, the saturation value of vertical stress does not decrease significantly.

Table I shows the fit parameters obtained for the Janssen's model. The α parameter is close to one, which indicates that the Janssen's predictions for the vertical stress are acceptable even for a silo with a slowly moving bottom. The K parameter, which represents the deflection of vertical to horizontal stress, varies and becomes smaller with a greater friction coefficient. These results are in agreement with the expected limits of K ; the system with $\mu = 0.0$ has a similar behavior to a liquid where the horizontal and vertical pressures are the same (Pascal's principle).

B. Varying the dispersity of radii

The vertical stresses σ_{zz} at the bottom for different dispersity of radii are displayed in Fig. 4. This change has no noticeable effect on the σ_{zz} profile, and Janssen's model fits well the averaged data of the simulations. This suggests that the Janssen's model is independent of the dispersity of the radii. It has been reported that the force chain length appears to be independent of the degree of polydispersity [28]. It is clear, however, that small dispersities may lead to crystallization, which could in principle give origin to different results. We obtained the scalar order parameter for a sixfold

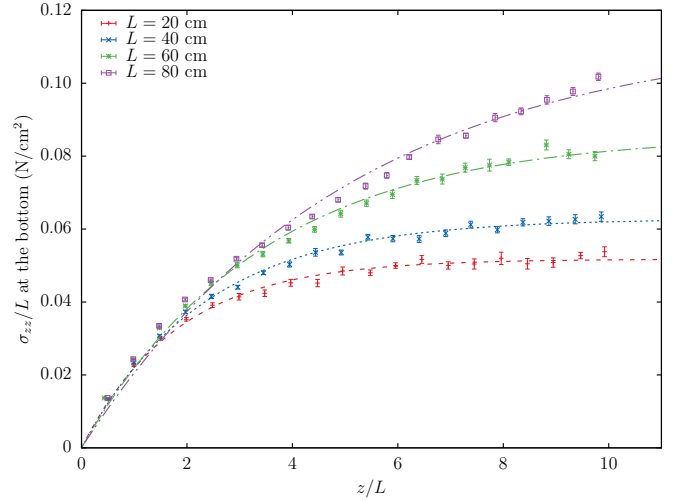


FIG. 5. Graphic for σ_{zz}/L as a function of the aspect ratio z/L of the column, where σ_{zz} is the vertical stress on the bottom for silos with $\mu = 0.6$ and different widths. The points are averages over 16 runs. The lines are the fits to the Janssen's model. This vertical stress in the bottom does not reach saturation for large values of L , even for columns with aspect ratio as large as 10. In general, the behavior becomes more hydrostatic as L grows. Full fit data in Table I.

symmetry $\psi_6 = |\langle e^{i6\theta_c} \rangle_c|$, and the average is taken over all contact directions θ_c in the neighborhood of a reference grain; the value of ψ_6 is 0.2 for smaller systems and decreases to 0.01 for larger systems, implying an almost complete lack of crystallinity in the column. The downward motion of the base tends to break the order in the silo.

Table I shows the fit parameters for different dispersity of radii. The system with greater dispersity of radii has a slightly larger K . If we consider the slight increase of the bulk density for higher values of ΔR , then these results disagree with

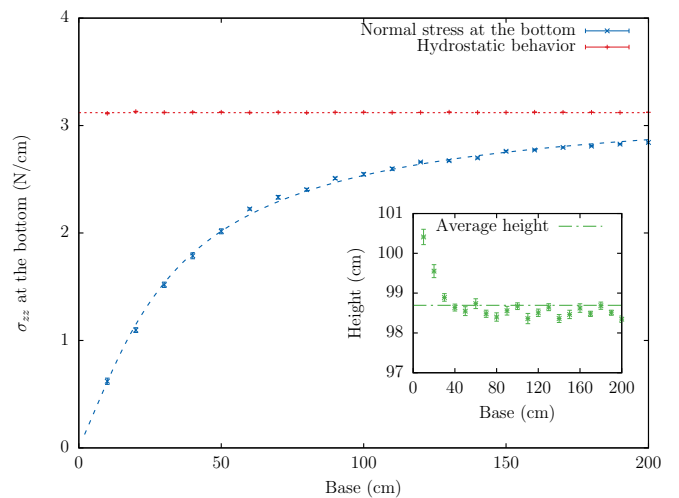


FIG. 6. Normal stress σ_{zz} at the bottom for silos with different bases but the same W/L ratio (W : weight, L : base size). In the inset we show the behavior of the column height for growing size of the base of the silo: for larger bases, some rearrangement of the disks reduces slightly this height. The solid line is the fit of Janssen's model with $\alpha = 1$, $K = 0.45 \pm 0.01$ and we used an average height of 98.7 cm.

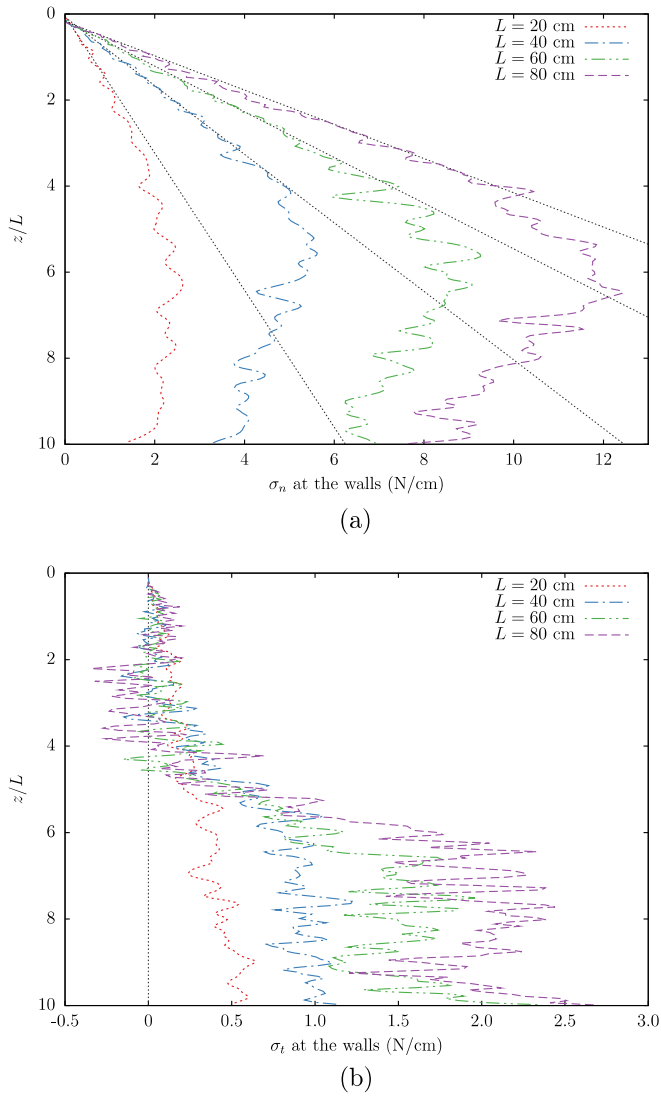


FIG. 7. (a) Normal and (b) tangential stress distributions on the walls, for different silo widths and keeping the aspect ratio fixed. The data were smoothed with Gnuplot using the “acsplines” option, where the standard errors of the data were used as smoothing weight. In (a), for larger silos ($L = 60$ and 80 cm) notice the quasilinear behavior on the upper half of the silo, similar to hydrostatic pressures (black dashed lines obtained using $\sigma_n = \rho_b g z$), confirming [6]. Notice in (b) the presence of negative tangential stress near the top of the column: there are related to the fact that on the bottom slides down, the walls “pull up” on the grains. Near the bottom, the weight of the column cancels this effect. In general, tangential stresses in the upper half of the silo are close to zero, confirming the observation of hydrostaticity.

[12,16], although the changes in bulk density are too small to imply an important difference.

C. Varying the silo width

In Fig. 5 we show σ_{zz}/L as a function of the aspect ratio z/L of the column for silos with different width. When this quantity increases, the Janssen’s model starts to lose relevance and the force propagation is decreased in the horizontal direction. Although the aspect ratio height to width is kept equal for all

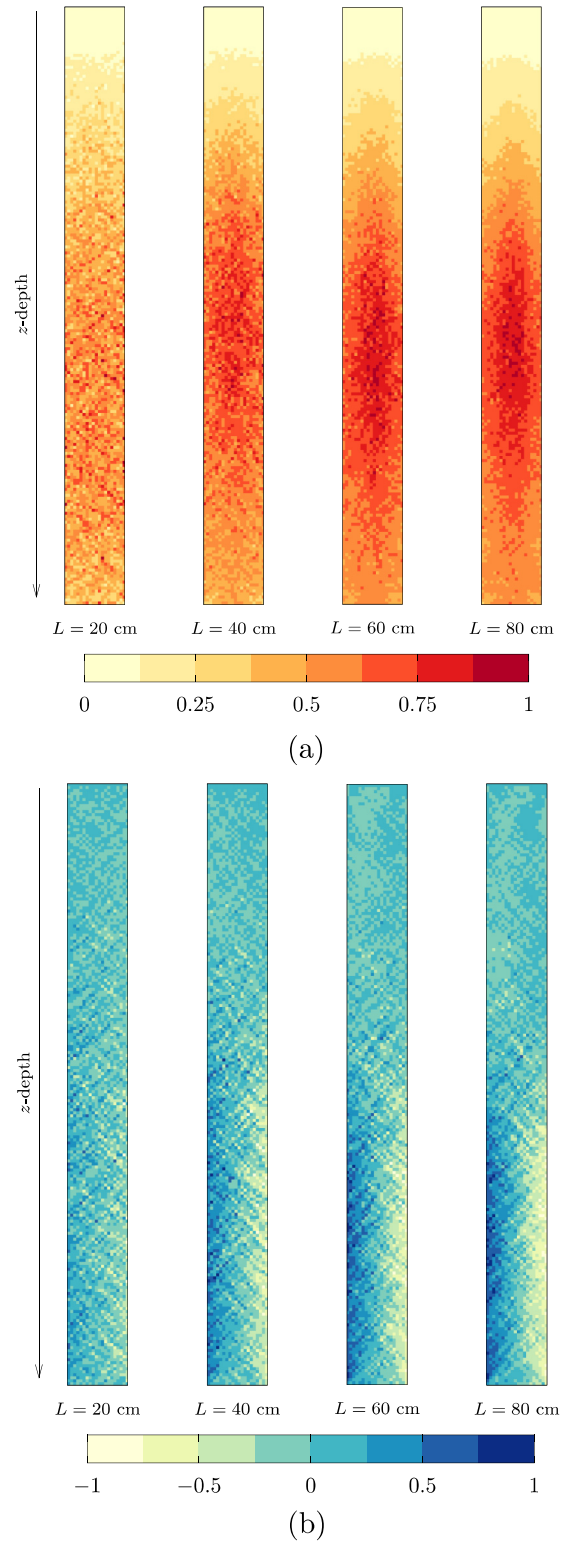


FIG. 8. Internal (a) normal and (b) tangential stress distributions for silos with 4000, 16 000, 36 000, and 64 000 grains keeping the aspect ratio fixed. The graphics are averages taken over 16 runs and normalized with the maximum values found in each case. Notice that for larger silos with aspect ratio fixed, the maximum normal stress appears at the center in the horizontal direction, and around a depth of $\sim 2/3z$. High tangential stress also tends to appear in chains, but small and mostly linear, forming an acute angle with the walls, similar to a herringbone pattern.

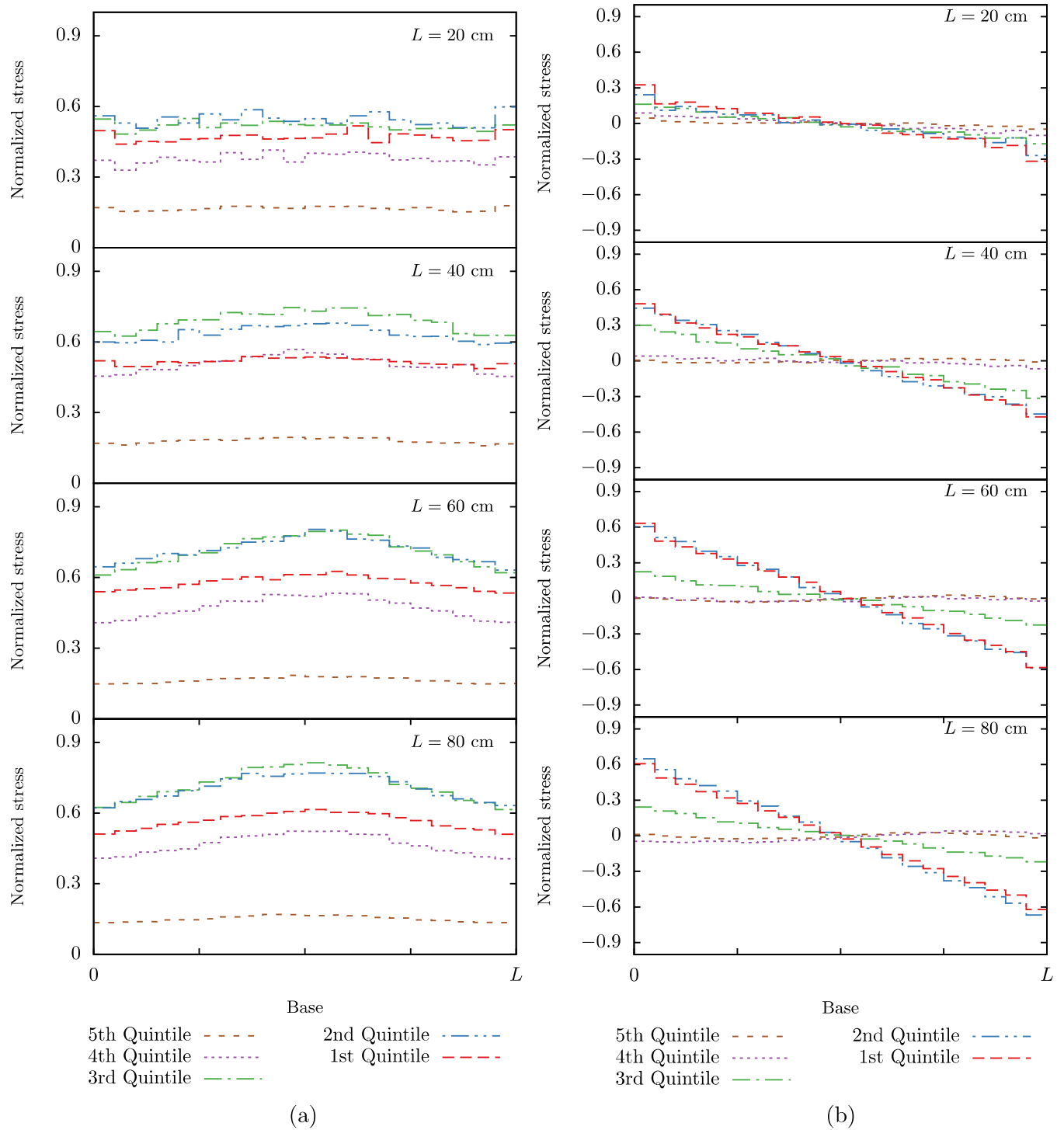


FIG. 9. Histograms of internal (a) normal and (b) tangential stress distributions along the horizontal width for four silos with $z/L = 10$. The first quintile corresponds to the bottom and the fifth quintile to the upper part. Notice how, as L grows, the internal normal stress concentrates around the center, in particular for grains in the second and third quintiles. For large L the system displays an inversion in the direction of the tangential stress since in the two lower quintiles this quantity goes from positive to negative going from left to right, but for the three higher quintiles the little variation one finds goes in the opposite direction.

systems, the silos with larger bases do not reach the saturation of vertical stress. As shown in Fig. 3, when the width increases (even with the aspect ratio z/L kept), the pressure at the bottom tends to a hydrostatic behavior. This indicates that for

larger systems the friction at walls plays a minor role for the determination of the pressure at bottom.

Table I shows the fit parameters for different silo widths. When the size of the base increases, the parameter K decreases

quickly, which suggests that the stress chains are not long enough to reach the walls and form stable arcs. The α parameter, as well as K , decreases when the size of the base increases. Since α is not included in the original model, its getting away from 1 can be thought as a failure of the model. On the other hand, a decrement in K and the general behavior observed in Fig. 5 are within the bounds of consistency of the model. However, the results indicate that for larger bases it becomes difficult for the model to fit the data.

In order to observe the behavior of the pressure at bottom when the width of the silo is increasing, in Fig. 6 we show simulations with the same W/L ratio, when W is the weight of the material. In principle, the pressure at bottom tends to a hydrostatic behavior with larger bases since the borders lose relevance. For larger bases, the friction between walls and grains is relevant only for narrow strips close to the walls. For this particular test, the Janssen’s model fits quite well the average data with values $\alpha = 1$ and $K = 0.45 \pm 0.01$.

The stress distribution on the walls was obtained by averaging several histograms generated for each time step. In Fig. 7 we show the normal and tangential stress distributions for silos of different sizes. For the protocol followed here, the maximum normal stress is around $\frac{2}{3}$ of the column height, measured from above, as can be clearly observed for the system with a large number of grains ($L = 80$ cm). We can see that near the surface of the silo the tangential stress changes direction (negative zone); this is associated to our moving-down-bottom protocol. The tangential stress is greater near the base, as expected from the fact that much of the weight of the granular column is carried by the lower half of the silo’s walls. If we observe the graphics in Fig. 7, we can note that Janssen’s model is not applicable in the upper half of the silo: in that zone, the normal stress on the walls has a hydrostatic behavior and the tangential stress is irrelevant. In the lower half of the silo, the tangential stress distribution tends to be homogenized while the normal stress distribution decreases; this suggests that K changes with the depth, that is, $K = K(z)$, at least for the larger systems.

To study the behavior of internal stress in the silos, we got the full stress tensor. Figure 8 shows the internal normal stress distributions (hydrostatic pressure) obtained using as a measure the quantity $(\sigma_{xx} + \sigma_{zz})/2$ and the internal tangential stress distributions obtained using as a measure the quantity $(\sigma_{xz} + \sigma_{zx})/2$. The graphics are normalized with the maximum values found in each case, which are, left to right, 3.8, 6.9, 11.0, and 15.0 N/cm, respectively, for Fig. 8(a), and 1.8, 2.0, 2.4, and 2.9 N/cm, respectively, for Fig. 8(b). For systems with greater number of grains, the maximum pressure is approximately in the middle of the silo, in the horizontal direction, and a bit below the middle in the z direction. The tangential stress at the walls is maximum in the lower half of the silo, as shown in Fig. 7(b). In general, near of the bottom the tangential stress is positive at the left and negative at the right, but in the upper half there is a slight inversion of signs.

It is convenient to observe the stress distribution along the width of the silos for different regions of the granular column. We divided the granular column into quintiles, each one covering an area of 20 cells wide and approximately 40 cells high, where the cells have the area A defined in Eq. (9); an average was made for each column in the quintile. Figure 9 shows the internal stress distributions along the

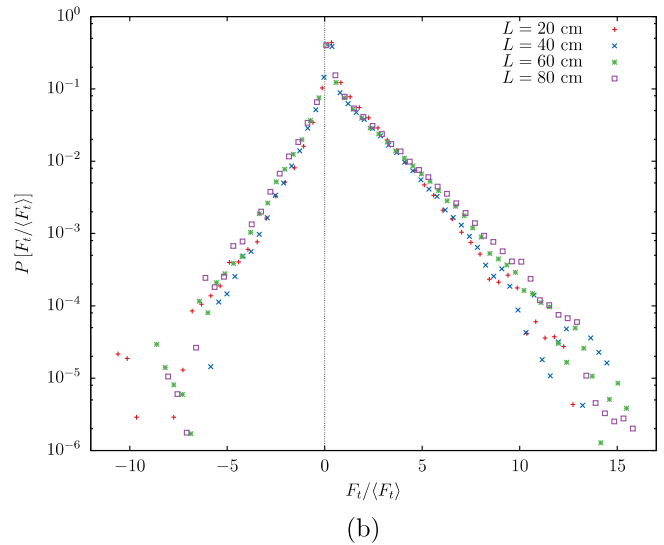
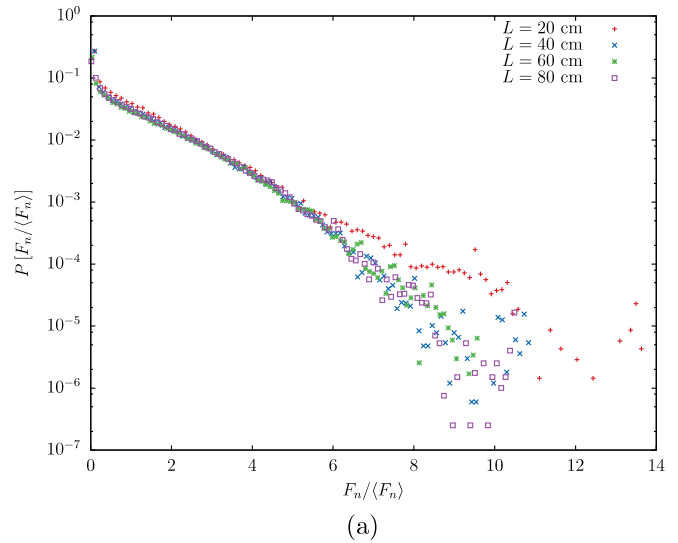


FIG. 10. Distribution of (a) normal and (b) tangential forces exerted at the walls for all times in simulations with a moving base. We observe the exponential decay in the frequency as F_n grows, regardless of the number of the grains. For normal forces very close to zero ($F_n / \langle F_n \rangle < 1$), the distribution shows a power law behavior. The tangential forces have a negative zone due to the moving base, but the negative forces have a minor range than the forces in the positive zone. The behavior is similar to the distribution of normal forces, showing an exponential decay for larger values of $|F_t|$, and a power law behavior for $|F_t| / \langle F_t \rangle < 1$.

horizontal direction for four silos with $z/L = 10$. The first quintile corresponds to the bottom and the fifth quintile to the upper part; in silos with larger bases, the difference is marked. For larger bases, the normal stress is greater in the middle of the base and it concentrates in the second and third quintiles. The silo with smallest base has a homogeneous distribution in the horizontal direction. The tangential stress is greater as it approaches the walls and concentrates in the first and second quintiles. In the remainder of the column, the distribution is slightly homogeneous. This suggests that part of the weight of the granular column is carried only by the lower walls where the friction plays an important role. In the upper walls, the

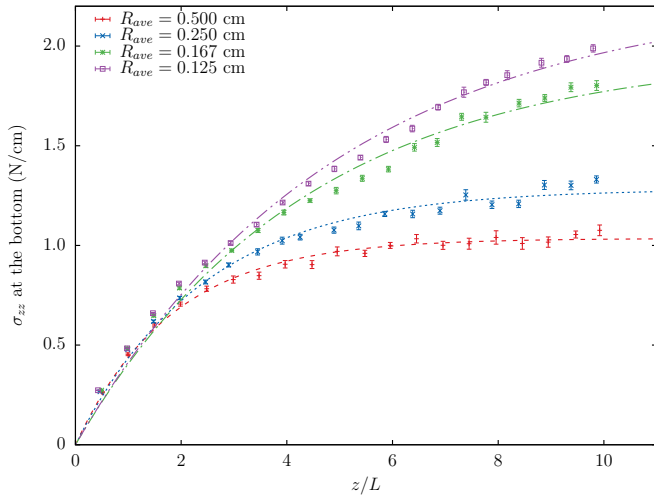


FIG. 11. Vertical stress σ_{zz} on the bottom for a silo of width $L = 20$ cm, with $\mu = 0.6$, and different values of average radii. The points are averages over 16 runs. The lines are the fits to the Janssen’s model. We can note the similarity with Fig. 5. Full fit data in Table I.

stress behavior seems to be hydrostatic, however, we observe a slight inversion of the signs with respect to that found for the lower walls.

Figure 10 shows the distribution of forces exerted at the walls. The distribution of forces seems to be independent of the friction coefficient, radii of dispersity, and base of the silo. We should notice the wide range of force amplitudes, reaching up to 15 times the mean force. The frequency for larger forces decays exponentially, but that for the low forces has a slight increase. This results are in agreement with the experiments carried out by Mueth *et al.* [29] where an empirical functional form that captures the exponential tail at large forces and the slight increase as forces decreased toward zero is proposed; however, no model predicts the distribution of forces yet. Currently, models are still being proposed [30].

D. Varying the average radii

The increase in hydrostaticity of the system as the size of the base of the silo increases (even when the aspect ratio z/L is kept fixed) suggests that a medium made with small particles (small with respect to the silo size) should start to derive from a pure Janssen’s behavior. The fundamental question here becomes the following: Does a medium of very small particles become hydrostatic, even if there still are tangential frictional forces? Notice that the presence of the constants g and t_{coll} means that there is no trivial scaling of dimensions on the system, and therefore one cannot use the results shown to predict in an easy way the behavior of silos with the same size but smaller (or larger) particles. Accordingly, we simulated silos with different grain average radii in a way similar to the simulations with different bases of silo, keeping the total mass in the silo constant. Figure 11 shows σ_{zz} at the bottom of the silo for different average radii with 20% of dispersity of the radii. If we compare with Fig. 5, we can note the loss of relevance (in the sense of approaching hydrostaticity) of the Janssen’s model when $R_{ave}/L < 0.008$.

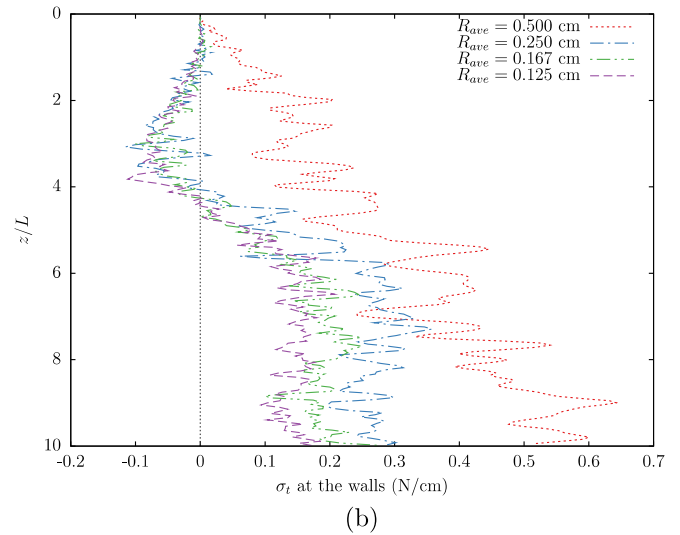
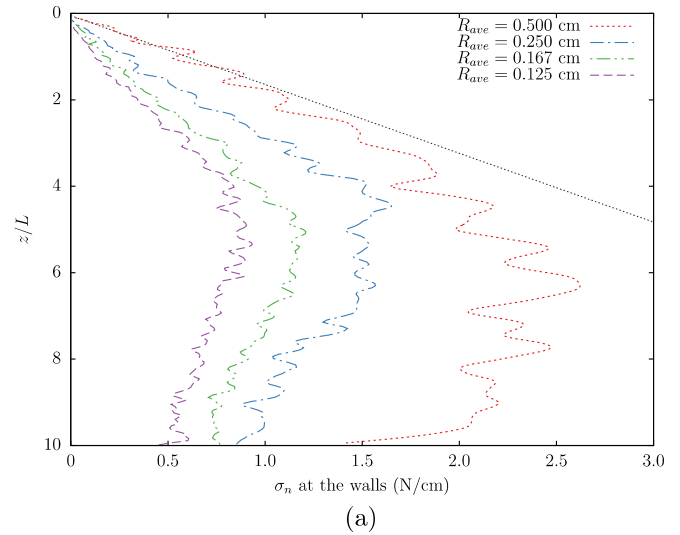


FIG. 12. Normal stress distribution on the walls, for different average radii but keeping the mass. The data were smoothed with Gnuplot using the “acsplines” option, where the standard errors of the data were used as smoothing weight. The black dashed line is the hydrostatic behavior of the pressure. When R_{ave} decreases, the normal stress on the walls decreases.

Table I shows the fit parameters for different average radii. We can note that the values of K and α are similar to those for silos with different bases, suggesting in this way that the same R_{ave}/L give the same behavior for the pressure on the bottom. Nevertheless, we find a very different behavior on the walls. Figure 12 shows the stress distributions on the walls for silos with grains of different average radii. The normal stress on the walls decreases as the average radius decreases; this can be attributed to strong force chains along the vertical direction which make the central part of the silo behave like a solid material with little horizontal deflection; likewise, it can be noted that K decreases as the average radius of the grains decreases, in accordance with the observation above. The tangential stresses on the walls for silos with particles of smaller average radii have almost the same behavior, indicating that the part of the weight of the material carried by the walls

saturates for $R_{\text{ave}}/L < 0.008$, and as before it is concentrated in the lower half of the silo height.

V. CONCLUSIONS

Simulations of two-dimensional silos filled with disks with different friction coefficients show a good fit to Janssen's model, reaching the saturation of normal stress on the base, as a result from the friction between grains and walls. These results are in general as expected, and a decrease in the friction coefficient tends to give a hydrostatic behavior. The value of K tends to one for smaller friction coefficients, and to zero for larger ones. The parameter α included in this work does not deviate much from 1, but a good fit requires $\alpha \leq 1$.

Varying the dispersity of radii has no significant effect, and Janssen's model seems independent of polydispersity. However, the model needs to be explored for a wider range of dispersity, and clearly no conclusions should be made about crystallizing cases.

When the aspect ratio height to width z/L is kept but the values of z and L are changed, the parameters K and α change strongly and, in principle, the Janssen's model loses relevance. These results seem to indicate that if $L \rightarrow \infty$, the pressure at bottom will be hydrostatic (even if the aspect ratio z/L is kept); the friction loses relevance. On the other hand, if z is kept and L increases, the normal stress at the bottom tends to its hydrostatic limit, agreeing closely to the small z/L limit of the Janssen's model. These results suggest that for larger systems (both in z and in L), the Janssen's model is less applicable.

In these simulations, when the base is moved downward, the walls are subject to greater normal stress in the middle of the granular column, and to greater tangential stress near the base,

and change of direction of the tangential stress near the surface. The internal stress distribution makes evident that the largest normal stress concentration is in the middle of the horizontal width and around $\frac{2}{3}$ of depth of granular column, measuring from the upper surface. The tangential stress is maximum near the walls and minimum in the middle of the horizontal width, and these effects are notorious for larger systems.

There are two very noteworthy findings in our simulations. The first one is the presence of internal avalanches in the silo, associated to the particular silo filling protocol used here, namely, the slow descent of the silo's bottom. We would like to remark again that these avalanches were beyond the sensitivity of the analogous experimental work [10]. One may also notice that, as expected, the slow descent of the bottom keeps the grain-wall tangential forces almost fully mobilized. A very intriguing problem is the statistics of the avalanches, which seem to vary widely in size. That will be considered in a future work. The second one is the similarity of behavior when increasing the base, keeping z/L fixed, with that obtained when decreasing the average radius, keeping the mass: both tend to the hydrostatic limits. The tangential stress on the walls seems to saturate if we decrease R_{ave} and the normal stress on the walls becomes smaller; this implies that the length of force chains does not reach the walls and most of the weight is supported by the middle part of the base.

ACKNOWLEDGMENTS

This work was performed in the hybrid cluster KUKULKAN-CONACYT (Grant No. CB-2015-252356) and the hybrid cluster ABACUS at Cinvestav. We acknowledge the help of J. L. Cabellos. This work was supported by the Project No. CB-82975 SEP-CONACYT.

-
- [1] A. Dogangun, Z. Karaca, A. Durmus, and H. Sezen, *J. Perf. Construct. Facil.* **23**, 65 (2009).
 - [2] H. M. Jaeger, S. R. Nagel, and R. P. Behringer, *Rev. Mod. Phys.* **68**, 1259 (1996).
 - [3] J. Kakalios, *Am. J. Phys.* **73**, 8 (2005).
 - [4] J. Duran, *Sands, Powders, and Grains: An Introduction to the Physics of Granular Materials* (Springer, New York, 2000).
 - [5] M. Sperl, *Granular Matter* **8**, 59 (2006).
 - [6] L. Vanel and E. Clément, *Eur. Phys. J. B* **11**, 525 (1999).
 - [7] P.-G. de Gennes, *Rev. Mod. Phys.* **71**, S374 (1999).
 - [8] L. Vanel, P. Claudin, J. P. Bouchaud, M. E. Cates, E. Clément, and J. P. Wittmer, *Phys. Rev. Lett.* **84**, 1439 (2000).
 - [9] J. W. Landry, G. S. Grest, and S. J. Plimpton, *Powder Technol.* **139**, 233 (2004).
 - [10] Y. Bertho, F. Giorgiutti-Dauphiné, and J.-P. Hulin, *Phys. Rev. Lett.* **90**, 144301 (2003).
 - [11] F. Vivanco, J. Mercado, F. Santibáñez, and F. Melo, *Phys. Rev. E* **94**, 022906 (2016).
 - [12] J. Lee, T. S. Yun, D. Lee, and J. Lee, *Soils Foundat.* **53**, 584 (2013).
 - [13] J. Horabik and R. Rusinek, *Int. Agrophys.* **16**, 23 (2002).
 - [14] R. Di Felice and C. Scapinello, *Granular Matter* **12**, 49 (2010).
 - [15] J. Wiącek and M. Molenda, *Int. J. Solids Struct.* **51**, 4189 (2014).
 - [16] J. Lopera Perez, C. Kwok, C. O'Sullivan, X. Huang, and K. Hanley, *Geotech. Lett.* **5**, 96 (2015).
 - [17] X. Gu, J. Hu, and M. Huang, *Granular Matter* **17**, 703 (2015).
 - [18] M. H. Khalili, J.-N. Roux, J.-M. Pereira, S. Brisard, and M. Bornert, *Phys. Rev. E* **95**, 032907 (2017).
 - [19] P. A. Cundall and O. D. Strack, *Geotechnique* **29**, 47 (1979).
 - [20] L. Brendel and S. Dippel, *Physics of Dry Granular Media*, NATO ASI Series Vol. 350 (Springer, Berlin, 1998), pp. 313–318.
 - [21] F. Gerl and A. Zippelius, *Phys. Rev. E* **59**, 2361 (1999).
 - [22] J. Schäfer, S. Dippel, and D. Wolf, *J. Phys. I* **6**, 5 (1996).
 - [23] G. Pérez, *Pramana* **70**, 989 (2008).
 - [24] K. Bagi, *Mech. Mater.* **22**, 165 (1996).
 - [25] B. Andreotti, Y. Forterre, and O. Pouliquen, *Granular Media: Between Fluid and Solid* (Cambridge University Press, Cambridge, 2013).
 - [26] A. Stukowski, *Modell. Simul. Mater. Sci. Eng.* **18**, 015012 (2009).
 - [27] A. Stukowski, OVITO—the open visualization tool, <http://ovito.org/>
 - [28] M. Muthuswamy and A. Tordesillas, *J. Stat. Mech.: Theor. Exp.* (2006) P09003.
 - [29] D. M. Mueth, H. M. Jaeger, and S. R. Nagel, *Phys. Rev. E* **57**, 3164 (1998).
 - [30] F. Radjai, *C. R. Phys.* **16**, 3 (2015).